the plant journal

SEB SOCIETY FOR EXPERIMENTAL BIOLOGY

The Plant Journal (2020) **103,** 379–394 doi: 10.1111/tpj.14736

Light controls stamen elongation via cryptochromes, phytochromes and COP1 through HY5 and HYH

Davide Marzi[1,2], Patrizia Brunetti[1], Giovanni Mele[3], Nadia Napoli[2], Lorenzo Calò[2], Erica Spaziani[2], Minami Matsui[4], Simone De Panfilis[5], Paolo Costantino[1,2], Giovanna Serino[2]* and Maura Cardarelli[1]*

[1]*IBPM-CNR c/o Sapienza Università di Roma, Roma, Italy,*
[2]*Dipartimento di Biologia e Biotecnologie Sapienza, Università di Roma, Roma, Italy,*
[3]*ISB-CNR, Monterotondo Scalo, Roma, Italy,*
[4]*RIKEN Center for Sustainable Resource Science, Yokohama, Kanagawa, 230-0045,Japan, and*
[5]*Centre for Life Nano Science, Istituto Italiano di Tecnologia, Viale Regina Elena, 291, Roma, I-00161, Italy*

Received 15 October 2019; revised 18 February 2020; accepted 27 February 2020; published online 6 March 2020.
*For correspondence (e-mails giovanna.serino@uniroma1.it; maura.cardarelli@uniroma1.it).

SUMMARY

In Arabidopsis, stamen elongation, which ensures male fertility, is controlled by the auxin response factor ARF8, which regulates the expression of the auxin repressor *IAA19*. Here, we uncover a role for light in controlling stamen elongation. By an extensive genetic and molecular analysis we show that the repressor of light signaling COP1, through its targets HY5 and HYH, controls stamen elongation, and that HY5 – oppositely to ARF8 – directly represses the expression of *IAA19* in stamens. In addition, we show that in closed flower buds, when light is shielded by sepals and petals, the blue light receptors CRY1/CRY2 repress stamen elongation. Coherently, at flower disclosure and in subsequent stages, stamen elongation is repressed by the red and far-red light receptors PHYA/PHYB. In conclusion, different light qualities – sequentially perceived by specific photoreceptors – and the downstream COP1–HY5/HYH module finely tune auxin-induced stamen elongation and thus male fertility.

Keywords: plant reproduction, light signaling, stamen, auxin, COP1, HY5, IAA19, phytochrome, cryptochrome, *Arabidopsis thaliana*.

INTRODUCTION

In self-pollinating plants such as *Arabidopsis thaliana*, stamen elongation is essential for male fertility as it is required to allow the transfer of mature pollen grains onto the pistil in open flowers.

In the stamen, pollen grains are formed and released in the apical part, the anther, while during stamen growth the radially structured filament provides mechanical support to the anther, serves as a conduit for water and nutrients, and anchors the stamen to the receptacle (Cardarelli and Cecchetti, 2014). In Arabidopsis, stamen growth is coordinated with pistil development to allow self-pollination, and consists of an early phase, when histo-specification and microsporogenesis occur, followed by a late phase, which includes elongation of stamen filaments, maturation of pollen grains, anther dehiscence and release of mature pollen grains at flower opening (anthesis) (Alvarez-Buylla *et al.*, 2010). Stamen filaments elongate slowly when the flower bud is closed (stages 10–11) and faster during flower disclosure (stages 12–13); after anthesis they continue to elongate until they become longer than the pistil at stage 14, when they reach their final length (Tashiro *et al.*, 2009). Filament cell elongation is triggered by auxin, which is synthesized in the anther tapetum during the early growth phase and subsequently transported to the filament during the late phase (Cecchetti *et al.*, 2008, 2015, 2017; Ghelli *et al.*, 2018). Among the different auxin response factors, ARF6 and ARF8 play a major role in stamen development (Nagpal *et al.*, 2005). Genetic and molecular evidence indicates that the splice variant products ARF8.4 and ARF8.2 have a specific effect on stamen elongation and directly activate the expression of *Aux/IAA19* (hereafter referred to as IAA19). In agreement, *IAA19* is expressed in stamens during late stamen development; the gain-of-function mutant of IAA19, *msg2-1*, is male sterile due to altered stamen elongation, while the loss-of-function mutant *msg2-21* is fertile due to defects in both stamen and pistil growth (Tashiro *et al.*, 2009).

Similarly, hypocotyl elongation also requires auxin-stimulated turnover of Aux/IAAs, such as IAA19 (Timpte *et al.*,

1992; Nagpal *et al.*, 2000; Tatematsu *et al.*, 2004; Chapman *et al.*, 2012). However, hypocotyl elongation is also heavily influenced by light, which affects auxin abundance and responsiveness: indeed, hypocotyls undergo an initial phase of cell elongation when the seedling is buried under the soil, followed by light-repressed growth upon its emergence (Huq, 2018). Two types of photoreceptors, phytochromes (PHYA–E) and cryptochromes (CRY1–2), are predominantly responsible for mediating light-controlled growth in hypocotyls (Sharrock and Quail, 1989; Ahmad and Cashmore, 1993; Nagatani *et al.*, 1993; Reed *et al.*, 1993; Clack *et al.*, 1994; Bruggemann *et al.*, 1996; Guo *et al.*, 1999). Downstream of the photoreceptors, CONSTITUTIVE PHOTOMORPHOGENIC 1 (COP1) (Deng *et al.*, 1991; McNellis *et al.*, 1994) represses light signaling by forming a COP1/SUPPRESSOR OF PHYA-105 (SPA) (Chen *et al.*, 2010) ubiquitin ligase and promoting proteolytic degradation of transcription factors such as ELONGATED HYPOCOTYL 5 (HY5) (Osterlund *et al.*, 2000), its homolog HYH (Holm *et al.*, 2002), LONG HYPOCOTYL IN FAR RED 1 (HFR1) (Yang *et al.*, 2005) and PHYTOCHROME INTERACTING FACTOR 3-LIKE 1 (PIL1) (Luo *et al.*, 2014). IAA19 has emerged as one of the key intersection nodes of light and auxin signaling in hypocotyls. In fact, PHYA, PHYB and CRY1 negatively affect auxin response by binding and stabilizing IAA19 and other Aux/IAAs (Reed *et al.*, 1998; Xu *et al.*, 2018; Yang *et al.*, 2018). COP1 promotes *IAA19* expression and induces hypocotyl elongation (Pacín *et al.*, 2016), while HY5 (and most likely also HYH) directly represses *IAA19* expression to inhibit hypocotyl elongation (Jing *et al.*, 2013). *IAA19* is also a direct target of PIL1 and HFR1, which act additively to repress *IAA19* transcription (Luo *et al.*, 2014). The relevance of this intersection between light and auxin for hypocotyl development is also indicated by the fact that both light and auxin pathways require the conserved protein complex COP9 signalosome (CSN) (Schwechheimer *et al.*, 2001; Franciosini *et al.*, 2013).

Here, by means of genetic, molecular and phenotypic analyses, we provide evidence for a role of light in controlling stamen elongation and male fertility during late flower development through the sequential perception of different light qualities by cryptochromes and phytochromes. Additionally, we demonstrate that, in analogy with hypocotyls, COP1 modulates auxin-induced stamen elongation through HY5, HYH and their target genes such as *IAA19*.

RESULTS

COP1 promotes elongation of stamen filaments

Since COP1 represses light-regulated hypocotyl development by promoting cell elongation (Deng *et al.*, 1991), we set out to assess if COP1 could also promote cell elongation in the stamen. To this end, we compared stamen filament length of the hypomorphic *cop1-4* and *cop1-6* mutant alleles (McNellis *et al.*, 1994) with their related wild type during late flower development (from stages 10 to 15), when stamen filament cell elongation accounts for 60–80% of the final stamen length (Figure 1). Stamen filaments (hereafter referred to only as filaments) from both *cop1* alleles were significantly shorter than the wild-type ones throughout stamen development (Figure 1b); in particular, at stage 14 when stamens reach their maximum length (Tashiro *et al.*, 2009), *cop1-4* and *cop1-6* filaments were respectively 13% and 16% shorter than the wild types. Flowers from both mutants were, however, still able to self-pollinate, albeit to a lesser extent, as *cop1* flowers yielded about 50% of the wild-type seed set (Figure S1a in the online Supporting Information). To investigate the causes of these phenotypical defects we first established a quantitative relationship between stamen and pistils in *cop1* mutants by plotting filament length as a function of pistil length at different developmental stages (stages 10–15) (Figure 1c). As expected, wild-type stamens were shorter than the pistil until anthesis and subsequently outgrew the pistil. In contrast, most *cop1-4* and *cop1-6* filaments were unable to outgrow the pistil throughout stamen development (Figure 1c), suggesting that the reduced stamen length could account for the smaller number of seeds set by these mutants. To confirm this hypothesis, we performed an *in vitro* germination assay on both *cop1-4* and *cop1-6* pollen grains, and we cross-pollinated wild-type pistils with *cop1-4* and *cop1-6* pollen grains (and vice versa). As shown in Figure S1(b), the pollen germination capacity of *cop1* mutants was comparable to that of the wild type, and siliques obtained by ♀wild type × ♂*cop1* crosses contained seed numbers comparable to that observed in siliques obtained by the reciprocal cross. Thus, the filament length defect, and not a reduction in pollen viability and/or ovule fertility, is responsible for the decreased fertility of *cop1* mutants.

To confirm that the difference in filament length between the wild type and *cop1* hypomorphs is due to a reduction in cell elongation, we compared the length of epidermal cells from wild-type, *cop1-4* and *cop1-6* filaments at stage 14. We found that mutant epidermal cells were on average 11% shorter than their wild-type counterpart, while no significant differences were observed in the number of filament epidermal cells among all genotypes (Table S1).

These results indicate that COP1 promotes stamen elongation by inducing filament cell expansion during late flower development.

COP1 acts through HY5 and HYH to promote filament elongation

To identify genes involved in COP1-mediated control of stamen elongation, we performed a transcriptomic

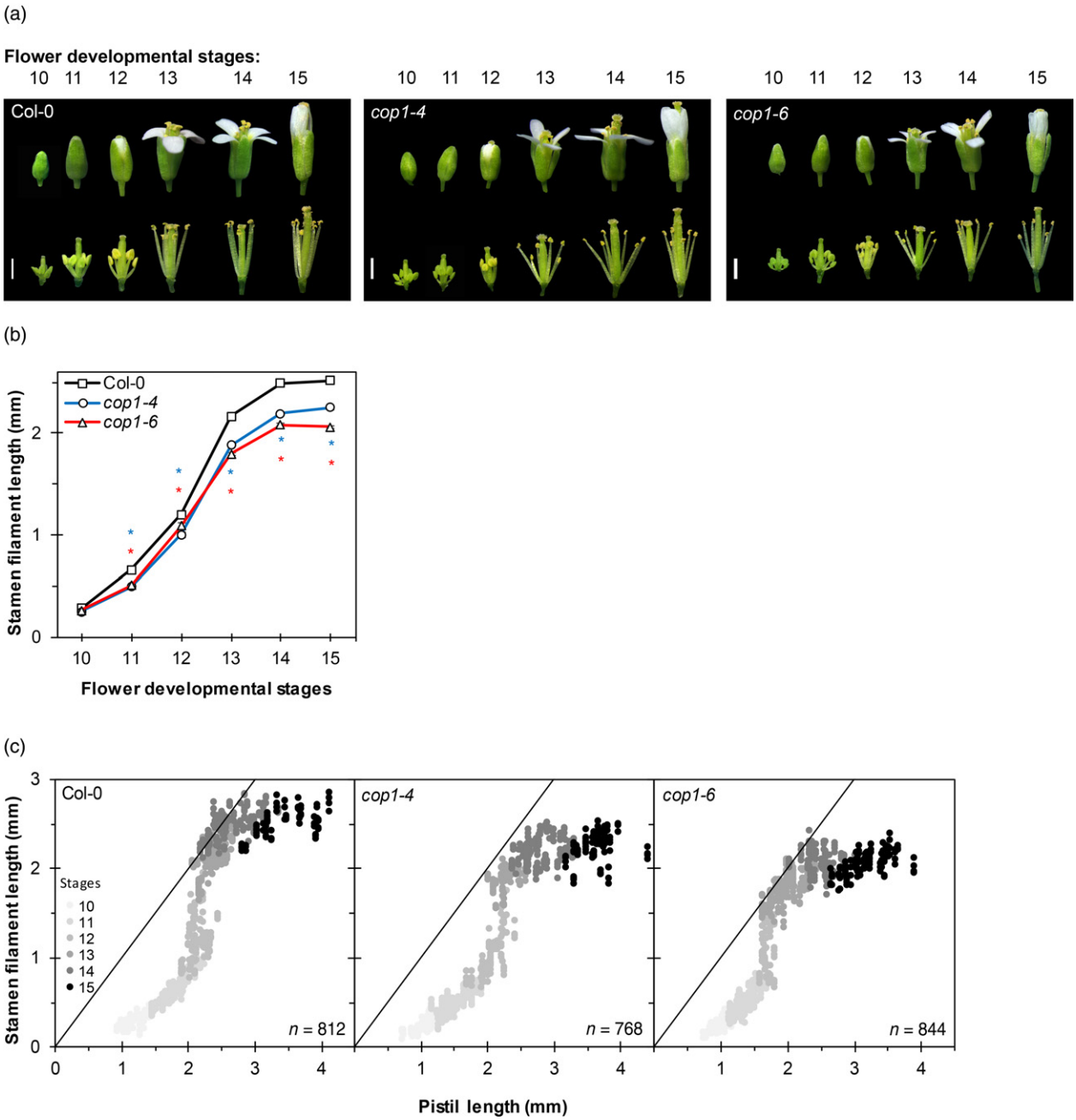

Figure 1. *cop1-4* and *cop1-6* mutant alleles exhibit short stamen filaments.
(a) Wild-type (Col-0), *cop1-4* and *cop1-6* flowers at stages 10–15. Top, whole flower; bottom, sepals and petals removed to show stamen length. Scale bar = 1 mm.
(b) Stamen filament elongation in wild-type (Col-0), *cop1-4* and *cop1-6* flowers at stages 10–15. Error bars are barely visible as they represent a low SEM value calculated from six independent plants (at least $n > 100$ per data point). Asterisks indicate a significant difference (at least $P < 0.05$) from the wild-type value at each specific stage, as determined by the two-tailed unpaired Student's *t*-test.
(c) Correlation between pistil and stamen length in wild-type (Col-0), *cop1-4* and *cop1-6* flowers. The length of the four long stamen filaments is plotted as a function of length of the pistil in each flower. Filaments longer than the pistil in each flower are located above the line drawn in each panel. Different stages are indicated by increasing grey intensities, from stage 10 (light grey) to stage 15 (black); *n* indicates the number of filaments measured per genotype.

analysis of wild-type Columbia-0 (Col-0) and *cop1-4* pooled dissected stamens at stages 10–12, when pre-anthesis filament elongation occurs.

Among 2208 differentially expressed genes, 1793 were found to be upregulated and 415 downregulated in the mutant (Table S2). Gene Ontology (GO) enrichment

analysis revealed that about 24% of the GO classification was related to responses to stimuli and included 'photoperception and response' as well as 'plant hormone regulation' (Figure S2). Several genes that are direct HY5 targets (Kurihara *et al.*, 2014), such as *RBCS1A* (RIBULOSE BISPHOSPHATE CARBOXYLASE SMALL CHAIN 1A), *RBCS1B* (RIBULOSE BISPHOSPHATE CARBOXYLASE SMALL CHAIN 1B) and *CHS* (CHALCONE SYNTHASE) were upregulated in *cop1-4* stamens, and this was confirmed by quantitative (q)RT-PCR analysis, pointing to an increased activity of HY5 due to lack of COP1 (Figure 2a), and suggesting that COP1 may promote stamen cell elongation by triggering degradation of HY5. Consistently, we found 97 genes that were oppositely regulated in *cop1-4* stamens and *hy5* seedlings (Chattopadhyay *et al.*, 1998; Kurihara *et al.*, 2014) (Table S3). In addition, both *HY5* and *HYH* transcripts were upregulated in *cop1-4* stamens (Figure 2b); as HY5 directly regulates *HYH* transcript levels as well as its own expression (Zhang *et al.*, 2017), it is conceivable that this upregulation could be due to the constitutive accumulation of HY5 and HYH observed in the *cop1* mutants (Osterlund *et al.*, 2000; Holm *et al.*, 2002).

To provide genetic evidence that HY5 and HYH are involved in stamen elongation, we compared filament length in flowers of the single null mutants *hy5-1*, *hyh* and of the double null mutant *hy5 hyh* (Figure S3a) with their respective wild types [Landsberg erecta (L*er*) and Wassilewskija (Ws)]. The Ws stamens had growth kinetics similar to, albeit slightly slower than, Col-0 stamens (Figure S3b). The L*er* stamens elongated slowly in the initial stages and later resumed a Col-0-like elongation (Figure S3b), resulting in a slight decrease in filament length during the final growth stages.

Growth kinetics of *hy5-1* and *hyh* filaments revealed a significant increase in their length in both single mutants (Figure 2c); this increase was observed from stages 12 to 15 for *hy5-1* (Figure 2d) and from stage 11 up to anthesis (stage 13) for *hyh* (Figure 2d). Interestingly, *hy5-1* and *hyh* filaments at stage 13 were respectively 10% and 15% longer, while *hy5 hyh* filaments were 40% longer than their wild-type control, pointing to an additive effect of the *hy5* and *hyh* mutations (Figure 2c,d). Furthermore, *hy5-ks50* and *hy5 hyh* flowers set a number of seeds comparable to their wild-type controls, while *hyh* flowers set a slightly (but significantly so) higher amount (Figure S3c). This difference between the double and single mutants can be explained by our observation that while lack of *HYH* triggers a faster stamen elongation but has no effect on pistil growth, mutations affecting both HY5 and HYH have a simultaneous effect on stamen and pistil growth. As a consequence, in the *hyh* mutant, stamens overgrow the pistil earlier, thus allowing self-fertilization to occur more efficiently (see Figure 2c,d). On the contrary, the normal seed set observed in the double mutant *hy5 hyh* might be due to stamens and pistils both growing longer than the wild type, thus allowing self-fertilization to occur normally.

All in all, these results indicate that HYH represses stamen elongation up to anthesis, while HY5 represses stamen elongation at and after anthesis, and suggest that the defect in stamen elongation observed in *cop1-4* mutants might be due to the increased stability of HY5 and HYH. To corroborate this notion, we compared filament length in the wild type (Col-0) and the *cop1-4 hy5-215* double mutant, hereafter referred to as *cop1 hy5*. Filament growth kinetics revealed that the *cop1 hy5* mutant exhibits significantly increased filament length at stages 13–15 (Figure 2e, f), a phenotype similar to the *hy5-1* mutant (compare Figure 2e,f with 2c,d), rather than to the short stamens of *cop1-4* (compare Figure 2e,f with Figure 1b,c). These results indicate that COP1 acts upstream of HY5 (and possibly to HYH) in stamens.

Figure 2. COP1 controls filament elongation through HY5.
(a), (b) Expression of *RBCS1A*, *RBCS1B* and *CHS* (a) and *HY5* and *HYH* (b) in pooled stamens at stages 10–12 from wild-type (Col-0) and *cop1-4* flowers, as determined by (q)RT-PCR. All cDNA levels were examined relative to the level of *ACTIN8* cDNA. Values are means ± SD of nine data points obtained from three biological replicates that were each analyzed in triplicate. Asterisks indicate a significant difference from the wild-type value (**$P < 0.01$, ***$P < 0.001$), as determined by the two-tailed unpaired Student's *t*-test.
(c) Correlation between pistil and stamen length in *hy5-1*, *hyh*, *hy5 hyh* and their relative wild-type controls (L*er*, and Ws). The length of the four long stamen filaments is plotted as a function of the length of the pistil in each flower. Filaments longer than the pistil in each flower are located above the line drawn in each panel. Different stages are indicated by increasing grey intensities, from stage 10 (light grey) to stage 15 (black); *n* indicates the number of stamens measured per genotype.
(d) Stamen filament elongation in *hy5-1, hyh* and *hy5 hyh* flowers at stages 10–15 compared with their related wild-type controls. Error bars are barely visible as they represent a low SEM value calculated from six independent plants (at least $n > 100$ per data point). Asterisks indicate a significant difference (at least $P < 0.05$) from the wild-type value at each specific stage as determined by the two-tailed unpaired Student's *t*-test.
(e) Correlation between pistil length and stamen filament length in the double mutant *cop1 hy5* and its relative wild-type control (Col-0). The length of the four long stamen filaments is plotted as a function of length of the pistil in each flower. Filaments longer than the pistil in each flower are located above the line drawn in each panel. Different stages are indicated by increasing grey intensities, from stage 10 (light grey) to stage 15 (black). *n* indicates the number of stamens measured per genotype.
(f) Stamen filament elongation in *cop1 hy5* flowers at stages 10–15 compared with its related wild-type control (Col-0). Error bars are barely visible as they represent a low SEM value calculated from six independent plants (at least $n > 100$ per data point). Asterisks indicate a significant difference (at least $P < 0.05$) from the wild-type value at each stage, as determined by the two-tailed unpaired Student's *t*-test.

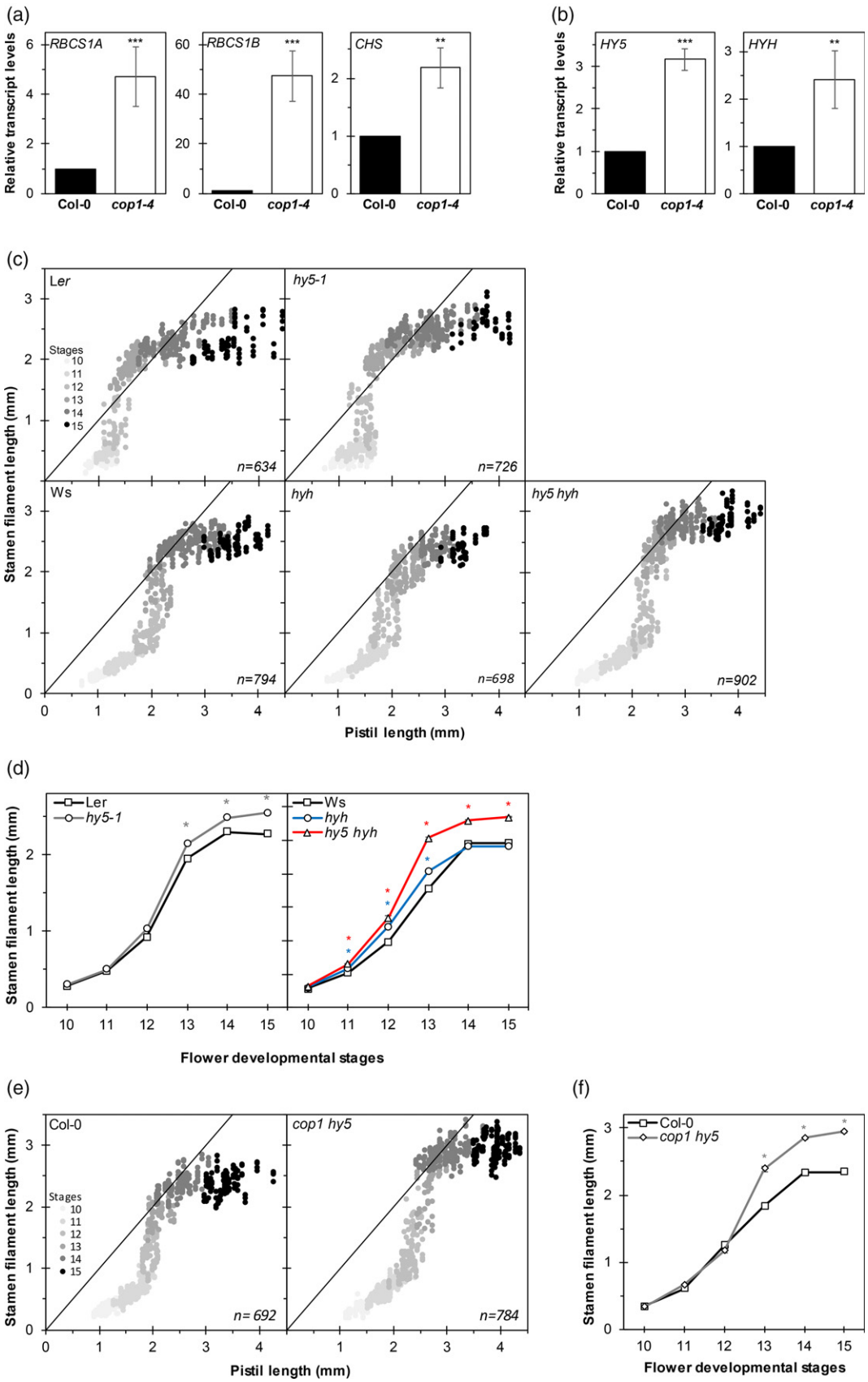

To assess whether two other well-known COP1 targets during hypocotyl growth, HFR1 and PIL1 (Yang *et al.*, 2005; Luo *et al.*, 2014), have a role in stamen elongation, we produced *hfr1 pil1* double mutants and compared their filament length with wild-type, *hfr1-4* and *pil1-1* flowers (Figure S4a). Filament growth kinetics from the wild type and single mutants were almost indistinguishable, while *hfr1 pil1* stamens exhibited a slight but significant decrease in filament length only at stage 15 (Figure S4b). These results indicate that HFR1 and PIL1 play only a marginal role during stamen elongation.

IAA19 acts downstream of *COP1* in stamens

In stamens, *IAA19* is involved in auxin-induced elongation and is directly regulated by two splice variants of *ARF8* (Ghelli *et al.*, 2018). In agreement, the dominant auxin-insensitive *massugu2* (*msg2-1*) allele of *IAA19,* which accumulates a stabilized form of IAA19, results in altered late stamen elongation which accounts for the male sterility and decreased seed production of this mutant line. In contrast, the *msg2-21* loss-of-function mutant is fertile and has a mild phenotype opposite to that of *msg2-1* (Tashiro *et al.*, 2009). As in hypocotyls, where the COP1–HY5 module regulates *IAA19* (Jing *et al.*, 2013; Pacín *et al.*, 2016), we hypothesized that this gene could act downstream of the COP1–HY5 module to also modulate stamen elongation. To validate this hypothesis, we first sought evidence for a possible alteration of *IAA19* expression in *cop1* stamens. Quantitative RT-PCR analysis on wild-type (Col-0) stamens indicated that *IAA19* is expressed at stages 10–12, and its expression further increases at stages 13 and 14 (Figure 3a). This expression profile is almost reversed in *cop1-4* stamens, where *IAA19* expression is lower than that of the wild type from stage 11 onwards (Figure 3b).

To support the notion that IAA19 acts downstream of COP1, we generated the *cop1 msg2* double mutant. We noticed that young adult plants at the F_2 generation showing a *cop1-4*-like phenotype included lines homozygous for *cop1-4* and containing the *msg2-1* mutation (Figure S5a). We selected lines homozygous for both mutations (Figure S5b,c) and compared their filament lengths with those of *cop1-4* and *msg2-1* single mutants. As shown in Figure 3(c), *msg2-1* stamens were consistently shorter than the pistil until stage 14, after which they continued elongating, reaching wild-type lengths at stage 15. Unlike *msg2-1* and similarly to *cop1-4*, *cop1 msg2* stamens show a reduced filament length throughout late flower development, without any further elongation at stage 15 (Figure 3c,d). In agreement, seeds set by the double mutant were comparable in number to those of *cop1-4* (Figure S1a). The phenotypic similarities between *cop1-4* and *cop1 msg2* stamens, as well as the lack of an additive effect of *msg2* and *cop1* mutations in the *cop1 msg2* double mutant, led us to conclude that COP1 and IAA19 act on a similar pathway, and suggest that HY5 and HYH, by repressing the transcription of *IAA19*, also prevent the accumulation of the more stable IAA19 protein MSG2-1. Indeed, *IAA19* transcript is less abundant in *cop1 msg2* than in *cop1-4* stamens (Figure 3e).

HY5 directly regulates *IAA19* expression in stamens

To assess whether COP1 controls *IAA19* transcription through HY5 and HYH, we first analyzed the *IAA19* expression level in *hy5 hyh* stamens and compared it with the corresponding wild type (Ws). We found that the expression pattern of *IAA19* in Ws stamens was comparable to that of Col-0, with the exception of stage 14 (compare Figure 4a with Figure 3a); in contrast, *IAA19* expression in *hy5 hyh* stamens showed a substantial increase at stages 11–13 compared with the wild type (Figure 4b). Accordingly, we found that *HY5* and *HYH* expression in the wild type decreased significantly at stages 11–12 (Figure 4c,d), the same stages in which *IAA19* expression is upregulated in *hy5 hyh* (compare Figure 4c,d with 4b). These results led us to conclude that HY5 and HYH repress *IAA19* expression in stamens during late flower development. To

Figure 3. COP1 control of filament elongation involves IAA19.

(a) *IAA19* expression in wild-type (Col-0) stamens at stages 10–14 as determined by (q)RT-PCR. *IAA19* cDNA levels were examined relative to the levels of *ACTIN8* cDNA. Values are means ± SD of nine data points obtained from three biological replicates that were each analyzed in triplicate. Asterisks indicate a significant difference (*$P < 0.05$, ***$P < 0.001$) from the value at stage 10, as determined by two-tailed unpaired Student's *t*-test.

(b) *IAA19* relative fold-change expression (qRT-PCR) in *cop1-4* stamens. Values are means ± SD of nine data points obtained from three biological replicates that were each analyzed in triplicate and were normalized to the values of the wild-type, set at 1 as indicated by the dashed line. Asterisks represent a significant difference (**$P < 0.01$, ***$P < 0.001$) from the wild-type value, as determined by the two-tailed unpaired Student's *t* test.

(c) Correlation between pistil and stamen length in *cop1-4, msg2-1* and *cop1 msg2* and their related wild-type (Col-0) controls. The length of the four long stamen filaments is plotted as a function of length of the pistil in each flower. Filaments longer than the pistil in each flower are located above the line drawn in each panel. Different stages are indicated by increasing grey intensities, from stage 10 (light grey) to stage 15 (black). *n* indicates the number of stamens measured per genotype.

(d) Stamen filament elongation in *cop1-4*, *msg2-1* and *cop1 msg2* flowers at stages 10–15 compared with their related wild-type controls (Col-0). Error bars are barely visible as they represent a low SEM value calculated from six independent plants (at least $n > 100$ per data point). Asterisks indicate a significant difference (at least $P < 0.05$) between the single and double mutant at each stage, as determined by the two-tailed unpaired Student's *t*-test.

(e) *IAA19* relative fold-change expression (qRT-PCR) in stamens at stages 10–14 from *cop1-4*, *msg2-1* and *cop1 msg2* flowers. Values are means ± SD of nine data points obtained from three biological replicates that were each analyzed in triplicate and were normalized to the values of the wild type, set at 1 as indicated by the dashed line. Asterisks or circles indicate a significant difference (*$P < 0.05$, ***$P < 0.001$, °$P < 0.05$) from the value of *cop1-4* or *msg2-1* respectively, at the same stage as determined by the two-tailed unpaired Student's *t*-test.

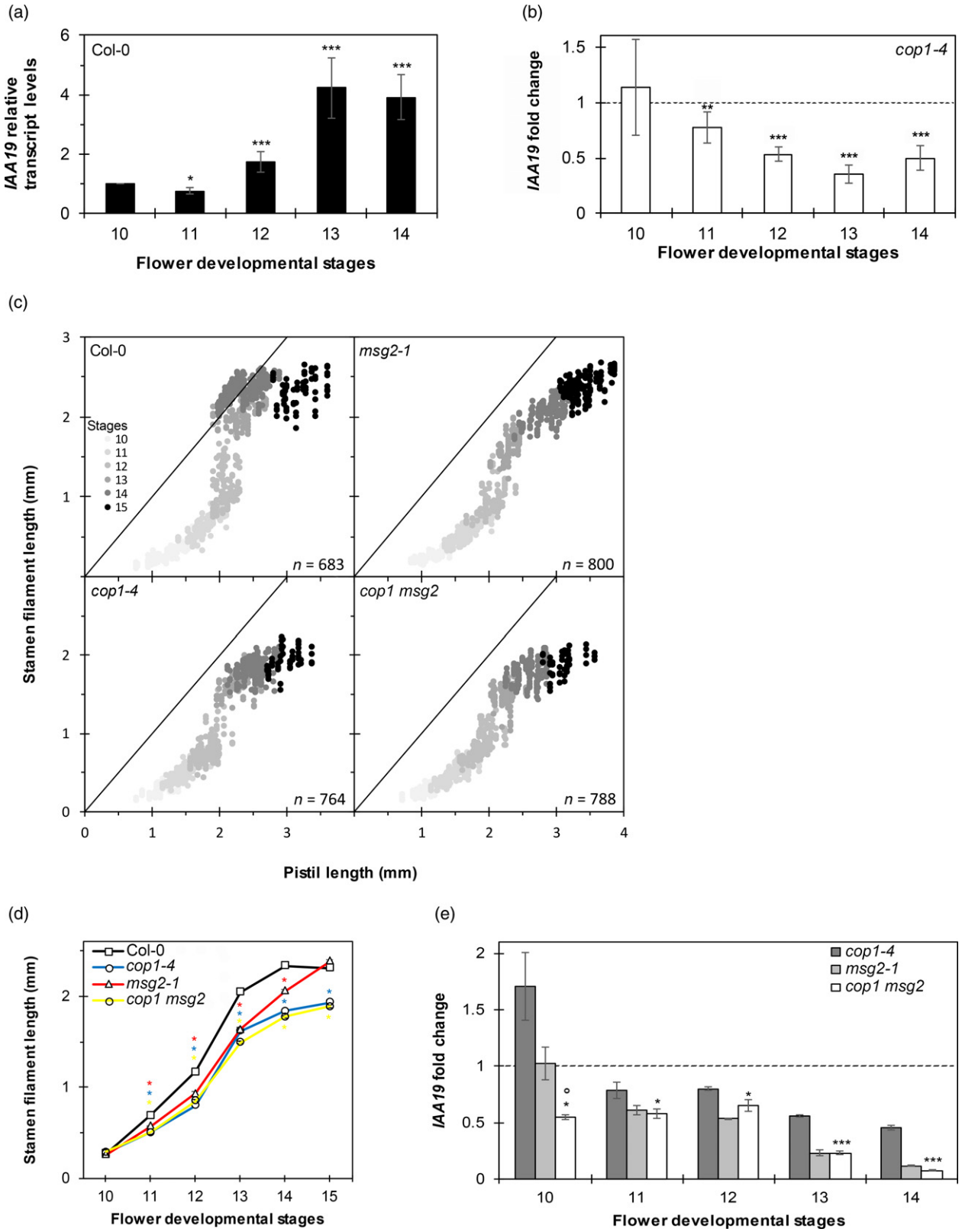

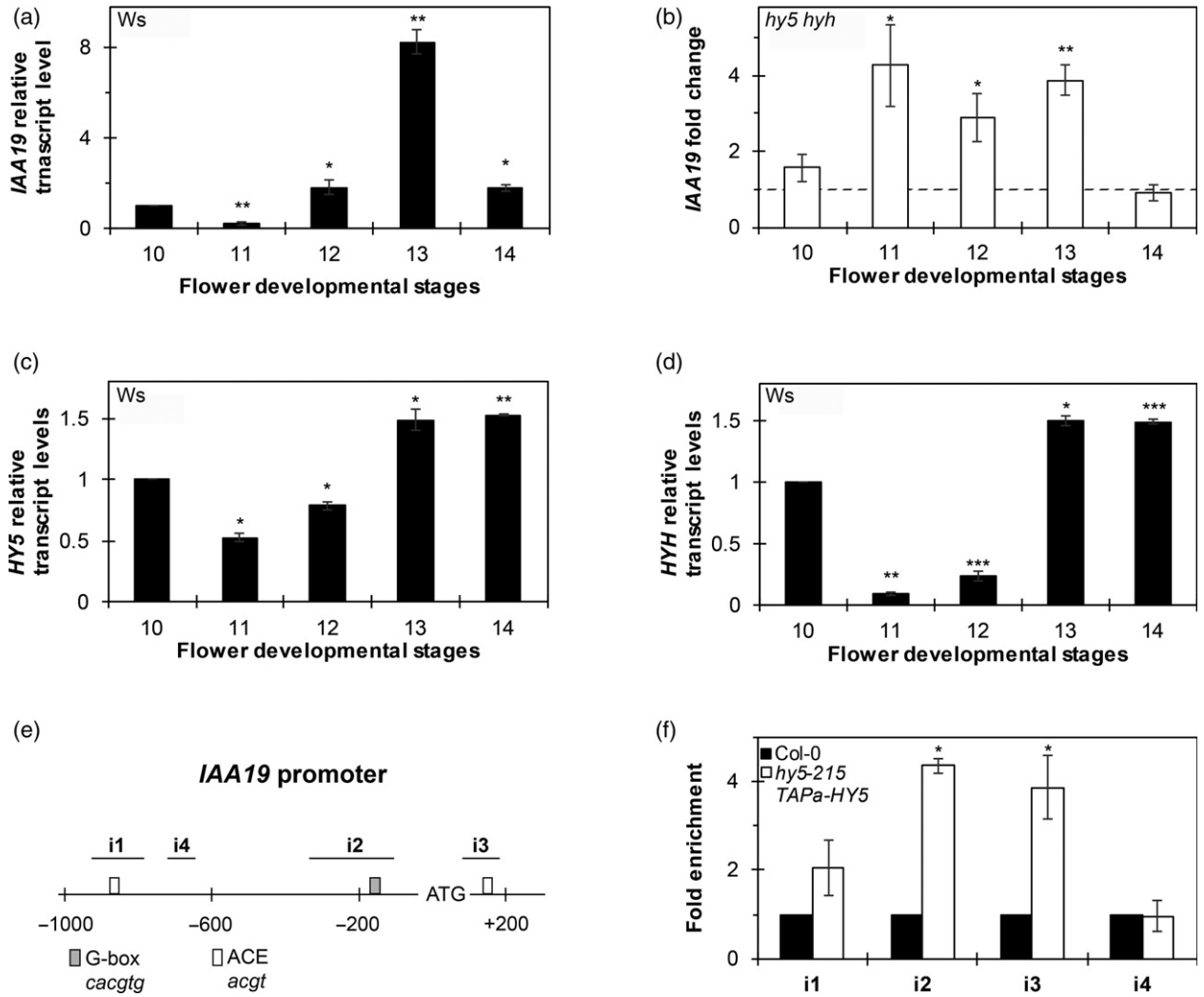

Figure 4. HY5 and HYH regulate *IAA19* expression.

(a) Expression of *IAA19* in stamens at stages 10–14 from wild-type (Ws) flowers as determined by (q)RT-PCR. *IAA19* cDNA levels were examined relative to the levels of *ACTIN8* cDNA. Values are means ± SD of nine data points obtained from three biological replicates that were each analyzed in triplicate. Asterisks indicate a significant difference (*$P < 0.05$, **$P < 0.01$) from the value at stage 10, as determined by the two-tailed unpaired Student's *t*-test.

(b) *IAA19* relative fold-change expression (qRT-PCR) in *hy5 hyh* stamens. Values are means ± SD of nine data points obtained from three biological replicates that were each analyzed in triplicate and were normalized to the values of the wild type, set at 1 as indicated by the dashed line. Asterisks represent a significant difference (*$P < 0.05$, **$P < 0.01$) from the wild-type value, as determined by the two-tailed unpaired Student's *t*-test.

(c), (d) Expression of *HY5* (c) and *HYH* (d) in stamens at stages 10–14 from wild-type (Ws) flowers as determined by (q)RT-PCR. *HY5* cDNA levels were examined relative to the levels of *ACTIN8* cDNA. Values are means ± SD of nine data points obtained from three biological replicates that were each analyzed in triplicate. Asterisks indicate a significant difference (*$P < 0.05$, **$P < 0.01$, ***$P < 0.001$) from the value at stage 10, as determined by the two-tailed unpaired Student's *t*-test.

(e) Schematic diagram of putative HY5 binding sites in the *IAA19* promoter. The upper black lines indicate fragments (i1, i2, i3, i4) amplified in the chromatin immunoprecipitation-qPCR assay.

(f) Chromatin immunoprecipitation analysis of TAPa–HY5 binding to the *IAA19* promoter. Chromatin immunoprecipitates were obtained from wild-type (Col-0) and *hy5-215* TAPa–HY5 inflorescences. Values are means ± SD of nine data points obtained from three biological replicates that were each analyzed in triplicate. Biological replicates were obtained by pooling inflorescences isolated from 50 independently grown plants for each genotype. Asterisks indicate a significant difference (*$P < 0.05$) from the wild-type value, as determined by the two-tailed unpaired Student's *t*-test.

establish whether HY5 directly regulates *IAA19* expression in stamens, we performed a chromatin immunoprecipitation (ChIP)-qPCR analysis to investigate the *in vivo* binding of HY5 to the *IAA19* promoter, using an overexpressing *HY5-TAPa* line (Rubio *et al.*, 2005) which expressed the HY5–TAPa fusion protein in inflorescences (Figure S6). HY5 directly binds target genes with a G-box (CACGTG) in their promoter sequence (Lee *et al.*, 2007; Jing *et al.*, 2013).

We and others have identified G-boxes and ACGT-containing elements (ACE) in the *IAA19* promoter (Lee *et al.*, 2007; Jing *et al.*, 2013; Ghelli *et al.*, 2018). In seedlings, HY5 binds to the G-box located between nucleotides −169 and −163 (I2) and to the ACE located between nucleotides +111 and +115 (i3). The results of the ChIP-qPCR analysis using primers specific for three regions containing G-box or ACE (Figure 4e), or a control which lacks HY5-specific recognition sequences (i4), showed that regions i2 and i3 were about four-fold enriched in *HY5-TAPa* flower buds while i4 was not enriched (Figure 4f). This result showed that HY5 – and likely also HYH – regulates *IAA19* expression by binding directly to its promoter. Thus, COP1 promotes stamen elongation by negatively acting on HY5 and HYH and on their capability to repress *IAA19* expression.

The direct repression effect of HY5 on *IAA19*, whose expression is instead promoted by ARF8.4 and ARF8.2 (Ghelli *et al.*, 2018), prompted us to assess if other stamen-expressed genes are co-regulated by HY5 and ARF8. We thus compared the *cop1-4* transcriptome with that of *arf8-7* (Ghelli *et al.*, 2018); this revealed that among the 382 differentially expressed genes in both mutants, 368 are concordant and only 14 display opposite expression (Table S4).

These data suggest that HY5 and ARF8 oppositely control the expression of a large subset of downstream genes involved in stamen development.

Photoreceptors have a negative affect on filament elongation

The involvement of COP1, HY5 and HYH in stamen elongation suggests that light may have a regulatory role in this process. The effect of *cop1* and *hy5 hyh* mutations on filament elongation from the inception of late development (stage 10) suggests that light may start to affect stamen growth when the flower bud is still closed. Indeed, our transcriptomic and (q)RT-PCR analyses indicate that *CRY1* and *CRY2*, as well as *PHYA*, are expressed in stamens at stages 10–12 (Figure S7). On the other hand, *PHYB* and *PHYE*, but not *PHYD*, are expressed in stamens at anthesis (Goosey *et al.*, 1997). To analyze the effect of cryptochromes and phytochromes on filament elongation, we measured filament length in the double mutants *cry1 cry2* and *phyA phyB* and in the triple mutant *phyB phyD phyE* (*phyBDE*) (Sharrock and Quail, 1989; Ahmad and Cashmore, 1993; Nagatani *et al.*, 1993; Reed *et al.*, 1993; Bruggemann *et al.*, 1996; Goosey *et al.*, 1997; Guo *et al.*, 1999). As shown in Figure 5(a,c), *cry1 cry2* filaments were longer (by up to 20%) than their wild-type counterparts from stage 10 to stage 12; they still exhibited an increased length, albeit to a lesser extent, at anthesis (11%) and at stage 14. Accordingly, *IAA19* transcript levels were significantly lower than in the wild type at stage 10 and slightly but significantly higher at stage 14 (Figure 5e). On the other hand, *phyA phyB* filaments were comparable to the wild type up to stage 11, while they exhibited an increased length (18% and 20% at stages 13 and 14, respectively) at subsequent stages (Figure 5b,d). Accordingly, *IAA19* transcript levels were significantly altered mainly from stages 12 to 14, in which they were up to four-fold higher than in the wild type (Figure 5f). Interestingly, *phyBDE* filament length was comparable to the wild type up to stage 12, while it was 13% shorter at subsequent stages (Figure 5b,d). Taken together, these results suggest that cryptochromes strongly repress stamen elongation when flower buds are still closed, while PHYA and PHYB repress stamen elongation mainly when flower buds are open. In addition, the comparison of the *phyA phyB* and *phyBDE* filament phenotypes suggests that PHYE may promote stamen elongation (Figure 5b,d). The altered expression of *IAA19* at stages in which *phyA phyB* filaments were longer than the wild type are in agreement with this phenotypical defect.

The long filament phenotype observed in *cry1 cry2* closed flower buds prompted us to assess whether light can penetrate through sepals and petals and reach the developing stamens. According to previous published data on flowers of the L*er* ecotype grown under continuous light (Smyth *et al.*, 1990), in closed flower buds stamens are shielded from light by the sepals up to stage 10, by sepals and partially by petals up to late stage 11 and by sepals and petals at stage 12, when flower buds start opening. To assess whether this also holds true for Col-0 flowers grown under long-day conditions, we analyzed flower buds from stages 10 to 13 before and after the removal of one sepal and one petal. As shown in Figure S8, in closed flower buds stamens are shielded by sepals at stage 10 and by sepals and petals at stage 11, while the apical region of the bud is only shielded by petals at stage 12. Thus, stamens are likely to be subjected to complex changes in light quality and intensity during their development in a similar fashion in L*er* and Col-0 ecotypes, with only a slight difference at stage 12, when part of the stamens is shielded only by petals in Col-0 while petals are still hidden by sepals in L*er*. Due to the complexity of our biological system, we could not test how monochromatic light conditions directly affect stamen development; however, we determined the absorption spectra of sepals and petals by collecting them from flower buds at different developmental stages and measured the absorption from 300 to 800 nm. The absorption spectrum of sepals was comparable to that reported for leaves (Shao *et al.*, 2008) with two major peaks in the blue and red wavelength regions and did not qualitatively change at different developmental stages (Figure 6a). Conversely, petals collected at stages 10–11 absorbed mainly blue light, while those collected from stages 12 to 14 absorbed all light wavelengths to the same extent, although an absorption preference for blue light was still observed (Figure 6b).

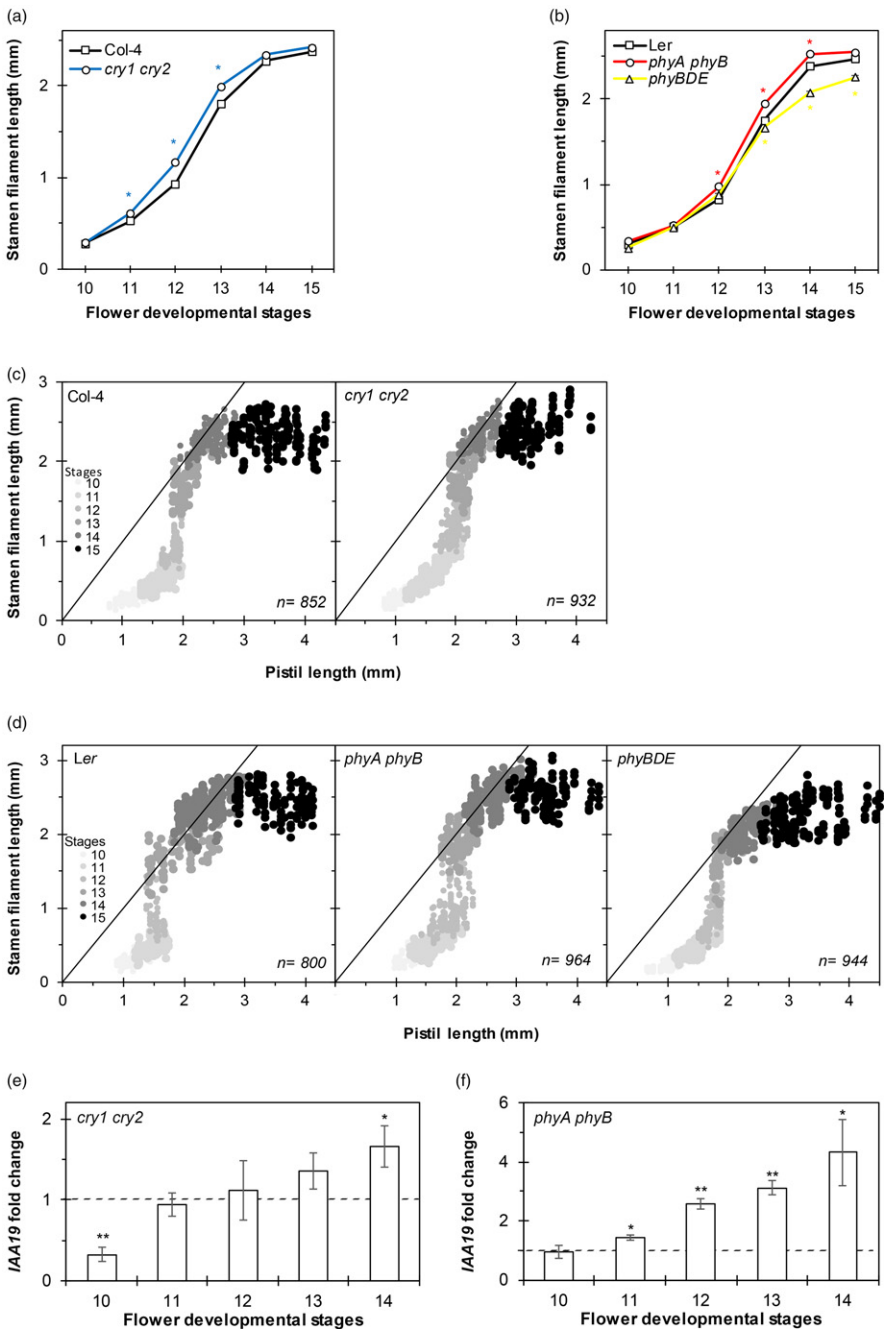

Figure 5. Cryptochrome and phytochrome mutations affect stamen filament elongation and *IAA19* expression.
(a), (b) Stamen filament elongation in *cry1 cry2* (a) and *phyA phyB* and *phyBDE* (b) flowers at stages 10–15 compared with their relative wild-type controls. Error bars are barely visible as they represent a low SEM value calculated from six independent plants (at least $n > 100$ per data point). Asterisks indicate a significant difference (at least $P < 0.05$) from the wild-type value at each stage, as determined by the two-tailed unpaired Student's *t*-test.
(c), (d) Correlation between pistil and stamen length in *cry1 cry2* (c) and *phyA phyB* and *phyBDE* (d) and their related wild-type controls. The length of the four long stamen filaments is plotted as a function of length of the pistil in each flower. Filaments longer than the pistil in each flower are located above the line drawn in each panel. Different stages are indicated by increasing grey intensities, from stage 10 (light grey) to stage 15 (black). *n* indicates the number of stamens measured per genotype.
(e), (f) *IAA19* relative fold change expression (qRT-PCR) in stamens at stages 10–14 from *cry1 cry2* (e) and *phyA phyB* (f) flowers. Values are means ± SD of nine data points obtained from three biological replicates that were each analyzed in triplicate and were normalized to the values of the wild type, set at 1 as indicated by the dashed line. Asterisks indicate a significant difference ($*P < 0.05$, $**P < 0.01$) from the wild-type value as determined by the two-tailed unpaired Student's *t*-test.

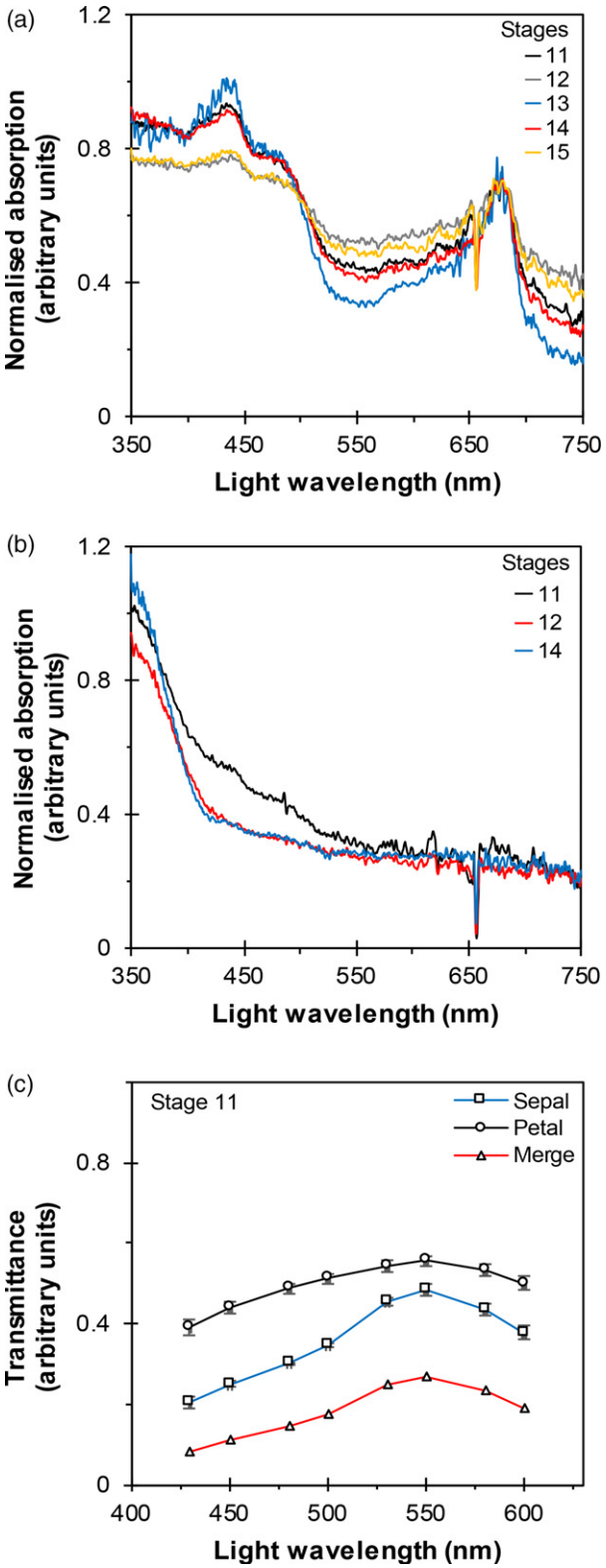

Figure 6. Sepals and petals shield blue and red light in flower buds.
(a) Absorption spectra of wild-type (L*er*) sepals from flower buds at stages 11–15 between 350 and 750 nm. Five different sepals per stage were detached from flowers and their absorption spectrum was determined.
(b) Absorption spectra of wild-type (L*er*) petals from flower buds at stages 11, 12 and 14 between 350 and 750 nm. Four different petals per stage were detached from flowers and their absorption spectrum was determined.
(c) Transmittance of light at discrete wavelengths of wild-type (L*er*) petals and sepals. Four petals or sepals were detached from flowers and their transmittance was determined. 'Merge' indicates light transmitted through sepals and petals. Values are means ± SD of three data points obtained from two biological replicates.

To determine the transmittance, i.e. the percentage of light that can penetrate through closed flower buds, we used a different experimental geometry in which we were able to measure both transmitted and forward-scattered light from petals and sepals at selected wavelengths. As shown in Figure 6(c), sepals at stages 10–11 selectively quenched blue and red light by 80% and 60%, respectively. Similarly, petals decreased transmittance of mainly blue and red light by 60% and 50%, respectively, at stages 10–11, while they decreased all other wavelengths to a similar minor extent (Figure 6c). These results strongly suggest that the amount of blue and red light reaching the stamens within stage 10 flower buds is severely curtailed and that it is further diminished at stage 11 due to the combined effect of petals and sepals, which are fully developed at this stage.

DISCUSSION

In previous work we have shown that stamen growth during late flower development is caused by auxin-driven filament cell elongation mediated by ARF8.4 and ARF8.2 splice variants (Ghelli *et al.*, 2018). Here, we report that light controls stamen elongation and that light and auxin signaling pathways intersect at IAA19 during late stamen development. Interestingly, IAA19 had also emerged as one of the intersection nodes of light and auxin signaling during hypocotyl cell elongation (Jing *et al.*, 2013; Pacín *et al.*, 2016).

Through the analysis of two different mutant alleles of the *COP1* light-repressor gene, we show that COP1 promotes stamen cell elongation via its targets HY5 and HYH. Indeed, *cop1-4* stamens are shorter than the wild type and accumulate transcripts known to be regulated by HY5 and HYH, while *hy5*/*hyh* single and double mutant stamens exhibit an opposite phenotype. HY5 and HYH seem to be the main effectors of COP1-mediated stamen elongation, since double mutant analysis shows that COP1 acts upstream of HY5, while HFR1 and PIL1, two additional targets of COP1 that are active in hypocotyl growth, play only a negligible role in stamen elongation. Additionally, by means of ChIP-PCR, qRT-PCR and genetic analysis, we provide several lines of evidence showing that the COP1–HY5/HYH module regulates *IAA19* expression. First, the *IAA19* transcript is oppositely expressed in *cop1-4* and *hy5 hyh* stamens; second, HY5 binds to the G-boxes in the *IAA19* promoter, as has also been previously shown for elongating hypocotyl cells; third, the phenotype of *cop1 msg2* stamens resembles that of *cop1*, indicating that that COP1 and IAA19 act on the same pathway. Indeed, comparison of *cop1-4* and *arf8-7* transcriptomes shows that, beside *IAA19*, a larger set of genes is concordantly regulated in the two

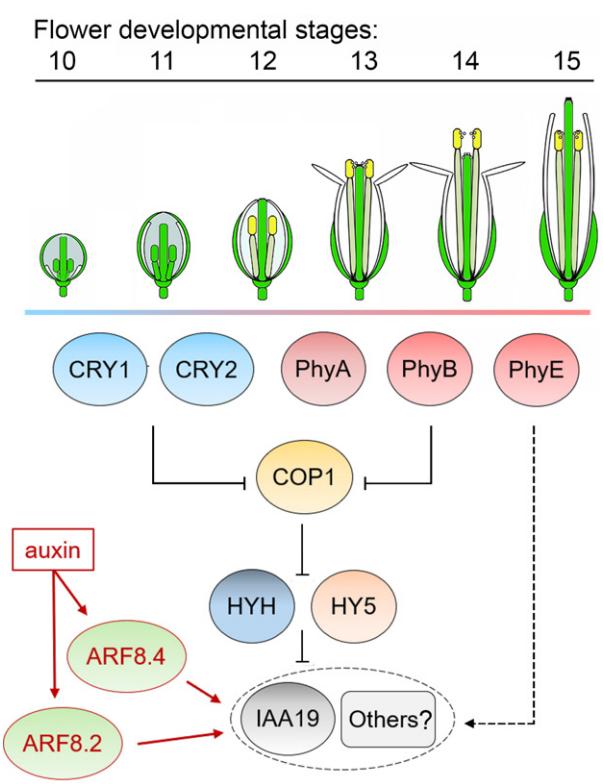

Figure 7. Model showing the role of photoreceptors and of the COP1–HY5/HYH module in stamen elongation before and after flower bud disclosure. Flower developmental stages are as described in Smyth *et al.* (1990). The colored line underneath the flowers indicates the stages in which CRY1/CRY2 (light blue) or PHYA/PHYB/PHYE (coral red) have an effect on stamen elongation according to their mutant phenotypes. The concomitant effect of auxin through ARF8 splice variants (ARF8.4 and ARF8.2) on *IAA19* expression is also shown (red lines and arrows).

mutants, suggesting a counteracting effect of ARF8 and HY5 on stamen development.

In Arabidopsis, COP1 and HY5/HYH activity is regulated by light through a wide range of photoreceptors. Here we found that light, acting sequentially through cryptochromes (CRY1 and CRY2) and phytochromes (PHYA and B), depending on the quality of the light perceived, affects stamen elongation most likely through the modulation of *IAA19* levels. Indeed, growth kinetics of *cry1 cry2* and *phyA phyB* stamens revealed that CRY1 and CRY2 repress filament elongation mainly in closed flower buds, while PHYA and PHYB repress filament elongation mainly in open flower buds. Further, altered *IAA19* expression correlates with the phenotypic defects observed in these mutants. Surprisingly, in *cry1 cry2* low levels of *IAA19* transcripts correlate with the slightly increased filament length at stages 10 and 11, when auxin concentration is high, while in *phyA phyB* (and in *cry1 cry2*) high levels of *IAA19* transcripts correlate with increased filament length at stages 13 and 14, when auxin concentration is almost undetectable (Aloni *et al.*, 2006; Cecchetti *et al.*, 2008, 2013).

Our results also suggest an opposite role of PHYE compared with PHYA and PHYB, as the *phyBDE* mutant exhibits shorter stamens at and after anthesis. As *PHYE*, similar to the auxin receptors *TIR1* and *AFB1* and to the auxin sensor *DR5*, is expressed in the junction region between filament and anther (Cecchetti *et al.*, 2008), which is involved in filament elongation, its promoting action on stamen elongation may possibly be correlated with auxin accumulation.

In closed flower buds, light is first shielded only by sepals (up to stage 10) and later by both sepals and petals (from stages 11 to 13) (this work). By spectrophotometric analysis we show here that sepals quench blue and, to a lesser extent, red light, while a further reduction in light intensity is caused by the additional shielding effect of petals. We have previously shown that stages 10 and 11 correspond to the 'slow' phase of stamen development, in which stamens elongate slowly (Ghelli *et al.*, 2018). The subsequent 'rapid' phase of stamen elongation occurs when the flower bud partially opens and is thus directly exposed to light (Smyth *et al.*, 1990). As shown in the model proposed in Figure 7, the initial slow stamen growth correlates well with the repression exerted by cryptochromes at these developmental stages. Once the flower bud has opened, phytochromes A and B start to negatively modulate stamen elongation up to stage 14. Their effect is possibly counteracted by the promoting effect of PHYE at the same stages. Indeed, indirect evidence that external light can modulate stamen elongation via phytochromes has been obtained by Brock and Weinig (2007), who showed an effect of different red:far-red ratios on stamen length.

Here, we show that light negatively modulates stamen elongation through the COP1–HY5/HYH module and that light and auxin pathways converge on *IAA19*, which therefore emerges as a marker of endogenous and environmental signals in stamens. This described effect of light reveals an additional function of the flower bud in 'selecting' the light quality perceived by the stamens and finely regulating stamen elongation, self-fertilization and seed yield.

Our findings thus show that the effect of light on growth by elongation occurs via a similar molecular module in stamens and in hypocotyls, although in the context of different signaling complexities. In hypocotyls, COP1 acts on several transcription factors and impinges on multiple Aux/IAA factors; in stamens, COP1 modulates auxin signaling by regulating a seemingly simpler set of factors which includes HY5 and HYH. Very recently, CRY1 (and PHYB) have been reported to interact directly with ARF8 (and ARF6) proteins to inhibit auxin-induced hypocotyl elongation (Mao *et al.*, 2020). Future work will reveal whether a similar mechanism exists in stamen. As the COP1–HY5/HYH module has been found to mediate thermomorphogenesis (Delker *et al.*, 2014) as well as photomorphogenesis (Ang *et al.*, 1998), our results provide crucial evidence supporting the notion that this module has been recruited multiple times during evolution to translate environmental stimuli into distinct developmental processes.

EXPERIMENTAL PROCEDURES

Plant materials and growth conditions

Arabidopsis thaliana mutant lines *cop1-4*, *cop1-6*, *hfr1-4*, *pil1-1*, *hfr1-4 pil1-1* (*hfr1 pil1*), *msg2-1*, *cop1-4 msg2-1* (*cop1 msg2*), *hy5-215* and *cop1-4 hy5-215* (*cop1 hy5*) are in the Columbia-0 (Col-0) background; *hy5-1*, *phyA-201 phyB-5* (*phyA phyB*) and *phyBDE* mutants are in the L*er* background; *hyh, hy5-ks50* and *hy5-ks50 hyh* (*hy5 hyh*) are in the Ws background; *cry1 cry2* is in the Columbia-4 (Col-4) background. The *hy5-215 TAPa-HY5* line is in the Col-0 background. Seeds were surface sterilized and stratified in the dark for 3 days at 4°C, then sown and grown on solid Murashige and Skoog medium supplemented with 1% sucrose for 10 days in a 16 h-light/8 h-dark cycle at 24/21°C with a light intensity of 130 μmol m^{-2} sec^{-1}. Seedlings were moved to pots containing soil and plants were grown in the same growth chamber until flowering (4 weeks).

Phenotypical and statistical analyses

Flower developmental stages were determined as previously described (Cecchetti *et al.*, 2008). For stamen growth kinetic analyses, about 200 flower buds from six independent plants per genotype were collected from stages 10 to 15. Petals and sepals were removed to measure stamen filament and pistil length. Filament length was determined as the distance from the base of the stamen filament to the base of the anther. Pistil length was determined as the distance from the base of the pistil to the tip of the stigma papillae. Images were acquired using a stereomicroscope (Carl Zeiss, https://www.zeiss.com/) equipped with a ProgRes C3 digital camera. The length of the four long stamen filaments and the pistil was measured using ImageJ (https://imagej.nih.gov/ij/).

Images of stamen filament cells were acquired with a light microscope (Motic BA410, https://www.motic.com/) equipped with

a ProgRes C3 digital camera. Cell length was measured using ImageJ.

Mean values were used to calculate the difference between mutant and wild-type stamens. *P*-values were determined by Student's *t*-test and differences were considered significant at $P < 0.05$. All graphs were generated with Excel. Differences in length smaller than 5% were considered as an effect of natural variation. A thin line is drawn in selected graphs passing through the graph origin with a slope of 45°. Filaments longer than the pistil in each flower are located above this line.

Seed set and pollen fertility analyses

To establish the seed set, we collected siliques from mutant lines and wild-type lines. We measured silique length and counted seed number for each silique. Mean values were used to calculate the difference between mutant and wild-type seed number. *In vitro* pollen germination assays were performed as previously described Cecchetti *et al.* (2013).

Generation of double mutants

To generate *cop1-4 msg2-1* (*cop1 msg2*), the parental lines *cop1-4* and *msg2-1* were manually cross-pollinated. F_1 heterozygous lines were propagated and F_2 seeds were harvested. Lines of the F_2 generation were screened phenotypically followed by derived cleaved amplified polymorphic sequencing (Neff *et al.*, 1998) to identify *cop1-4 msg2-1* homozygous lines as previously described, using dCAPS Finder 2.0 (http://helix.wustl.edu/dcaps/) to select primer sequences and restriction enzymes. The *Mse*I and the *Cla*I restriction enzymes (Takara, https://www.takarabio.com/), were used to digest *cop1-4* and *msg2-1* amplification products, respectively.

To generate *hfr1-4 pil1-1* (*hfr1 pil1*), the parental lines *hfr1-4* (Salk_037727) and *pil1-1* (SAIL_438_C01) were manually cross-pollinated. F_1 heterozygous lines were propagated and F_2 seeds were harvested. F_2 lines were screened through PCR to identify *hfr1 pil1* homozygous lines, which contain a T-DNA insertion in both *hfr1-4* and *pil1-1*. The primers used are listed in Table S5.

Immunoblot analysis

Protein extracts from inflorescences were prepared using a previously described extraction buffer (Franciosini *et al.*, 2015) with minor modifications [extraction buffer 50 mM TRIS–HCl pH 7.5, 150 mM NaCl, 4 M urea, 0.1% Nonidet P-40, 10 mM EDTA pH 8, 1 mM phenylmethylsulfonyl fluoride and 1× plant protease inhibitor cocktail (Sigma, https://www.sigmaaldrich.com/)] and subjected to immunoblot analysis with an anti-Myc antibody (Sigma). Immunoreactive bands were detected using enhanced chemiluminescence (Clarity Western ECL blotting substrate; Bio-Rad, https://www.bio-rad.com/). Signals were detected with a ChemiDoc XRS imaging system and analyzed with the ImageLab software (Bio-Rad).

Preparation of RNA sequencing samples, sequencing, and data mining

For each genotype, total RNA was extracted from pooled dissected stamens at stages 10, 11 and 12, ensuring that all three stages were equally represented. Two biological replicates were collected. Total RNA extraction was performed using an RNeasy Plant Mini Kit (Qiagen, https://www.qiagen.com/). The RNA quality was tested using a 2100 Bioanalyzer (Agilent, https://www.agilent.com/). Illumina TruSeq cDNA libraries were prepared and sequenced in 50-bp paired ends on an Illumina HiSeq 2000 platform (https://www.illumina.com/). The paired-end reads were aligned to the TAIR10 reference transcriptome using Bowtie 2.2.7 (http://bowtie-bio.sourceforge.net/bowtie2/index.shtml). The Bowtie output was elaborated by SAMtools 0.1.19 (http://samtools.sourceforge.net) to obtain the number of mapped reads for each gene. The expression level of each transcript was measured by the RPKM (reads per kilobase of transcript, per million mapped reads) method. To identify differentially expressed genes, minimum read number and minimum fold change were used as parameters. The minimum read number to pass the cut-off was imposed to be more than five times the gene length. The minimum fold change was calculated as the ratio between the minimum RPKM value between the two repetitions of the *cop1-4* and the maximum RPKM value of the two repetitions of the wild type. Only those genes that had a minimum fold change ≥ 1.7 were considered to be differentially expressed. The GO terms were directly associated with the genes analyzed with VirtualPlant 1.3 (http://virtualplant.bio.nyu.edu/cgi-bin/vpweb/) (Katari *et al.*, 2010) and those with a *P*-value ≤ 0.01 were considered as enriched.

Quantitative RT-PCR

(q)RT-PCR was carried out as previously described (Cecchetti *et al.*, 2013; Franciosini *et al.*, 2013). About 150 stamens were sampled per stage from stages 9 to 14; total RNA was extracted using an RNeasy Plant Mini Kit (Qiagen) and reverse-transcribed using a QuantiTect Reverse Transcription Kit (Qiagen). SYBR Green-based quantitative assays were performed by using a Rotor-Gene Q and analyzed using Rotor-Gene Q 2.3.1 software. Each PCR reaction was run in technical triplicates and repeated three times with two different preparations of cDNA. Gene expression levels were normalized to the levels of *ACTIN8*. The primers used in these experiments are listed in Table S5.

Chromatin immunoprecipitation-qPCR assay

The ChIP-qPCR procedure was performed on 35-day-old inflorescences as previously described (Jing *et al.*, 2013; Ghelli *et al.*, 2018), with some modifications. Flower bud tissue (300–600 mg) was cross-linked to DNA with formaldehyde. The chromatin was sonicated to obtain an average DNA fragment size between 0.3 and 0.8 kb. The sonication efficiency was checked. Salmon sperm/protein A beads were used to pull-down TAPa-HY5 proteins contain an IgG in the tag, linked to chromatin. The ChIP-qPCR products were used for (q)RT-PCR using the primers listed in Table S5. Three independent biological replicates were performed for statistical significance.

Sepals and petal absorption and transmittance measurements

Petals and sepal absorption was measured using an AvaLight-DHS deuterium lamp coupled to an AvaSpec-2048 spectrometer (Avantes BV, https://www.avantes.com/) through multimode optical fibers. Detached petals and sepals were held close to the tip of the lamp fiber and the transmitted light was focused on the fiber directed to the spectrometer. Measurements were collected via the AvaSoft – Basic Software (Avantes BV). Absorption spectra for all the samples were obtained as the logarithmic ratio between the light intensities transmitted by the true samples and an empty sample, both subtracted by a background electronic signal. Absorption was measured for wavelengths in the 300–800 nm interval.

Transmittance was measured illuminating detached petals or sepals at different developmental stages by light from a 300 W

Lambda XL Xe lamp (Sutter Instruments, https://www.sutter.com/) coupled with a VF5 tunable filter wheel (Sutter Instruments). Transmitted and forward-scattered light was recorded by a 10 mm × 10 mm aperture PD300 photodiode (Ophir Photonics, https://www.ophiropt.com/) with automatic background subtraction.

ACCESSION NUMBERS

The RNA sequencing (RNA-seq) data sets have been deposited in the National Center for Biotechnology Information Sequence Read Archive database (http://www.ncbi.nlm.nih.gov) under BioProject accession number PRJNA576031. The *arf8-7* stamen RNA-seq dataset has been published under BioProject accession number PRJNA383483 (Ghelli *et al.*, 2018). The data set for the microarray analysis in wild-type and *hy5*-1 seedlings has ben published under accession number GSE62119 (Kurihara *et al.*, 2014).

ACKNOWLEDGEMENTS

We thank Dr Monica Carabelli (IBPM-CNR, Italy), Dr Kotaro Yamamoto (Hokkaido University, Japan), Dr Vicente Rubio (CNB, Spain), Dr Ning Wei (Yale University, USA) and Dr Jorge Casal (Universidad de Buenos Aires, Argentina). This work was partially supported by a research grant to MC and GS from the Italian Ministry of Foreign Affairs (Direzione Generale per la Promozione del Sistema Paese) and by a research grant to PC, GS and MC from the Italian Ministry of Education, University and Research (Progetti di Ricerca di Interesse Nazionale). We wish to thank Miguel Blazquez, Gloria Coruzzi and Ning Wei for insightful discussions.

AUTHOR CONTRIBUTIONS

Conceptualization and methodology: MC and GS. Investigation, validation and formal analysis: DM, LC, PB, ES, NN and SDP. Data curation: GM. Writing (original draft): MC, DM and GM. Visualization: DM. Writing (review and editing): GS and PC. Funding acquisition: MC, GS and PC. Supervision: MC and DM.

CONFLICT OF INTEREST

The authors declare that they have no conflicts of interest.

DATA AVAILABILITY STATEMENT

The authors confirm that all experimental data are available and accessible via the main text and/or the Supporting Information or from the National Center for Biotechnology Information Sequence Read Archive database (see above).

SUPPORTING INFORMATION

Additional Supporting Information may be found in the online version of this article.

Figure S1. Seed set and pollen germination capacity in single and double mutants of *COP1*, *HY5*, *HYH* and *IAA19*.

Figure S2. Gene Ontology term enrichment analysis for biological process of *cop1-4* differentially expressed genes.

Figure S3. *hy5* and *hyh* mutant alleles exhibit long stamen filaments.

Figure S4. *hfr1* and *pil1* mutants have a marginal role in stamen filament elongation.

Figure S5. Young adult *cop1 msg2* plants exhibit a *cop1-4* phenotype.

Figure S6. The TAPa–HY5 protein is expressed in the inflorescences of *hy5-215*.

Figure S7. Expression of *CRY1*, *CRY2* and *PHYA* in wild-type stamens.

Figure S8. Wild-type (Col-0) flowers at stages 10–13.

Table S1. Comparison of the length and number of epidermal cells from wild-type (Col-0), *cop1-4* and *cop1-6* stamens at stage 14.

Table S2. Reads per kilobase of transcript per million mapped reads of each gene in the two biological replicas from wild-type and *cop1-4* pooled stamens at stages 10–12.

Table S3. Oppositely expressed genes in *cop1-4* stamens and *hy5* seedlings.

Table S4. Differentially co-expressed or oppositely expressed genes in *cop1-4* and *arf8-7* pooled stamens at stages 10–12.

Table S5. List of primers used in this study.

REFERENCES

Ahmad, M. and Cashmore, A.R. (1993) *HY4* gene of *A. thaliana* encodes a protein with characteristics of a blue-light photoreceptor. *Nature*, **366**, 162–166.

Aloni, R., Aloni, E., Langhans, M. and Ullrich, C.I. (2006) Role of auxin in regulating Arabidopsis flower development. *Planta*, **223**, 315–328.

Alvarez-Buylla, E.R., Benítez, M., Corvera-Poiré, A. *et al.* (2010) Flower development. *Arabidopsis Book*, **8**, e0127.

Ang, L.-H., Chattopadhyay, S., Wei, N., Oyama, T., Okada, K., Batschauer, A. and Deng, X.-W. (1998) Molecular Interaction between COP1 and HY5 defines a regulatory switch for light control of Arabidopsis development. *Mol. Cell*, **1**, 213–222.

Brock, M.T. and Weinig, C. (2007) Plasticity and environment-specific covariances: an investigation of floral-vegetative and within flower correlations. *Evolution*, **61**, 2913–2924.

Bruggemann, E., Handweger, K., Essex, C. and Storz, G. (1996) Analysis of fast neutron-generated mutants at the *Arabidopsis thaliana HY4* locus. *Plant J.* **10**, 755–760.

Cardarelli, M. and Cecchetti, V. (2014) Auxin polar transport in stamen formation and development: how many actors? *Front. Plant Sci.* **5**, 1–13.

Cecchetti, V., Altamura, M.M., Falasca, G., Costantino, P. and Cardarelli, M. (2008) Auxin regulates Arabidopsis anther dehiscence, pollen maturation, and filament elongation. *Plant Cell*, **20**, 1760–1774.

Cecchetti, V., Altamura, M.M., Brunetti, P., Petrocelli, V., Falasca, G., Karin, L., Costantino, P. and Cardarelli, M. (2013) Auxin controls Arabidopsis anther dehiscence by regulating endothecium lignification and jasmonic acid biosynthesis. *Plant J.* **74**, 411–422.

Cecchetti, V., Brunetti, P., Napoli, N., Fattorini, L., Altamura, M.M., Costantino, P. and Cardarelli, M. (2015) ABCB1 and ABCB19 auxin transporters have synergistic effects on early and late Arabidopsis anther development. *J. Integr. Plant Biol.* **57**, 1089–1098.

Cecchetti, V., Celebrin, D., Napoli, N., Ghelli, R., Brunetti, P., Costantino, P. and Cardarelli, M. (2017) An auxin maximum in the middle layer controls stamen development and pollen maturation in Arabidopsis. *New Phytol.* **213**, 1194–1207.

Chapman, E.J., Greenham, K., Castillejo, C., Sartor, R., Bialy, A., Sun, T.-P. and Estelle, M. (2012) Hypocotyl transcriptome reveals auxin regulation of growth-promoting genes through GA-dependent and -independent pathways. *PLoS ONE*, **7**, e36210.

Chattopadhyay, S., Ang, L., Puente, P., Deng, X. and Wei, N. (1998) Arabidopsis bZIP Protein HY5 directly interacts with light-responsive promoters in mediating light control of gene expression. *Plant Cell*, **10**, 673–683.

Chen, H., Huang, X., Gusmaroli, G. *et al.* (2010) Arabidopsis CULLIN4-Damaged DNA Binding Protein 1 Interacts with CONSTITUTIVELY PHOTOMORPHOGENIC1-SUPPRESSOR OF PHYA complexes to regulate photomorphogenesis and flowering time. *Plant Cell*, **22**, 108–123.

Clack, T., Mathews, S. and Sharrock, R.A. (1994) The phytochrome apoprotein family in Arabidopsis is encoded by five genes: the sequences and expression of PHYD and PHYE. *Plant Mol. Biol.* **25**, 413–427.

Delker, C., Sonntag, L., James, G.G.V. *et al.* (2014) The DET1-COP1-HY5 pathway constitutes a multipurpose signaling module regulating plant photomorphogenesis and thermomorphogenesis. *Cell Rep.* **9**, 1983–1989.

Deng, X., Caspar, T. and Quail, P.H. (1991) *cop1*: a regulatory locus involved in light-controlled development and gene expression in Arabidopsis. *Genes Dev.* **5**, 1172–1182.

Franciosini, A., Lombardi, B., Iafrate, S. *et al.* (2013) The Arabidopsis COP9 SIGNALOSOME INTERACTING F-BOX KELCH 1 protein forms an SCF ubiquitin ligase and regulates hypocotyl elongation. *Mol. Plant*, **6**, 1616–1629.

Franciosini, A., Moubayidin, L., Du, K. *et al.* (2015) The COP9 SIGNALOSOME is required for postembryonic meristem maintenance in *Arabidopsis thaliana*. *Mol. Plant*, **8**, 1623–1634.

Ghelli, R., Brunetti, P., Napoli, N. *et al.* (2018) A newly identified flower-specific splice variant of AUXIN RESPONSE FACTOR8 regulates stamen elongation and endothecium lignification in Arabidopsis. *Plant Cell*, **30**, 620–637.

Goosey, L., Palecanda, L. and Sharrock, R.A. (1997) Differential patterns of expression of the Arabidopsis PHYB, PHYD, and PHYE phytochrome genes. *Plant Physiol.* **115**, 959–969.

Guo, H., Duong, H., Ma, N. and Lin, C. (1999) The Arabidopsis blue light receptor cryptochrome 2 is a nuclear protein regulated by a blue light-dependent post-transcriptional mechanism. *Plant J.* **19**, 279–287.

Holm, M., Ma, L.G., Qu, L.J. and Deng, X.W. (2002) Two interacting bZIP proteins are direct targets of COP1-mediated control of light-dependent gene expression in Arabidopsis. *Genes Dev.* **16**, 1247–1259.

Huq, E. (2018) Direct convergence of light and auxin signaling pathways in Arabidopsis. *Mol. Plant*, **11**, 515–517.

Jing, Y., Zhang, D., Wang, X., Tang, W., Wang, W., Huai, J., Xu, G., Chen, D., Li, Y. and Lin, R. (2013) Arabidopsis chromatin remodeling factor PICKLE interacts with transcription factor HY5 to regulate hypocotyl cell elongation. *Plant Cell*, **25**, 242–256.

Katari, M.S., Nowicki, S.D., Aceituno, F.F. *et al.* (2010) VirtualPlant: a software platform to support systems biology research. *Plant Physiol.* **152**, 500–15.

Kurihara, Y., Makita, Y., Kawashima, M., Hamasaki, H., Yamamoto, Y.Y. and Matsui, M. (2014) Next-generation sequencing of genomic DNA fragments bound to a transcription factor in vitro reveals its regulatory potential. *Genes (Basel)*, **5**, 1115–1131.

Lee, J., He, K., Stolc, V. *et al.* (2007) Analysis of transcription factor HY5 genomic binding sites revealed its hierarchical role in light regulation of development. *Plant Cell*, **19**, 731–749.

Luo, Q., Lian, H., He, S., Li, L., Jia, K. and Yang, H.Q. (2014) COP1 and phyB physically interact with PIL1 to regulate its stability and photomorphogenic development in Arabidopsis. *Plant Cell*, **26**, 2441–2456.

Mao, Z., He, S., Xu, F. *et al.* (2020) Photoexcited CRY1 and phyB interact directly with ARF6 and ARF8 to regulate their DNA-binding activity and auxin-induced hypocotyl elongation in Arabidopsis. *New Phytol.* **225**(2): 848–865. https://doi.org/10.1111/nph.16194.

McNellis, T.W., Arnim, A.G.Von, Araki, T., Komeda, Y. and Mis, S. (1994) Genetic and molecular analysis of an allelic series of *copl* mutants suggests functional roles for the multiple protein domains. *Plant Cell*, **6**, 487–500.

Nagatani, A., Reed, J.W. and Chory, J. (1993) Isolation and initial characterization of Arabidopsis mutants that are deficient in Phytochrome A. *Plant Physiol.* **102**, 269–277.

Nagpal, P., Ellis, C.M., Weber, H., *et al.* (2005) Auxin response factors ARF6 and ARF8 promote jasmonic acid production and flower maturation. *Development*, **132**, 4107–4118.

Nagpal, P., Walker, L.M., Young, J.C., Sonawala, A., Timpte, C., Estelle, M. and Reed, J.W. (2000) AXR2 encodes a member of the Aux/IAA protein family. *Plant Physiol.* **123**, 563–573.

Neff, M.M., Neff, J.D., Chory, J. and Pepper, A.E. (1998) dCAPS, a simple technique for the genetic analysis of single nucleotide polymorphisms: experimental applications in *Arabidopsis thaliana* genetics. *Plant J.* **14**, 387–392.

Osterlund, M.T., Hardtke, C.S., Ning, W. and Deng, X.W. (2000) Targeted destabilization of HY5 during light-regulated development of Arabidopsis. *Nature*, **405**, 462–466.

Pacín, M., Semmoloni, M., Legris, M., Finlayson, S.A. and Casal, J.J. (2016) Convergence of CONSTITUTIVE PHOTOMORPHOGENESIS 1 and PHYTOCHROME INTERACTING FACTOR signalling during shade avoidance. *New Phytol.* **211**, 967–979.

Reed, J.W., Nagpal, P., Poole, D.S., Furuya, M. and Chory, J. (1993) Mutations in the gene for the Red/Far-Red Light receptor Phytochrome B alter cell elongation and physiological responses throughout Arabidopsis development. *Plant Cell*, **5**, 147–157.

Reed, J.W., Elumalai, R.P. and Chory, J. (1998) Suppressors of an *Arabidopsis thaliana* phyB mutation identify genes that control light signaling and hypocotyl elongation. *Genetics*, **148**, 1295–1310.

Rubio, V., Shen, Y., Saijo, Y., Liu, Y., Gusmaroli, G. and Dinesh-kumar, S.P. (2005) An alternative tandem affinity purification strategy applied to Arabidopsis protein complex isolation. *Plant J.* **41**, 767–778.

Schwechheimer, C., Serino, G., Callis, J., Crosby, W.L., Lyapina, S., Deshaies, R.J., Gray, W.M., Estelle, M. and Deng, X. (2001) Interactions of the COP9 signalosome with the E3 ubiquitin ligase SCF TIR1 in mediating auxin response. *Science*, **292**, 1379–1383.

Shao, L., Shu, Z., Peng, C., Lin, Z. and Yang, C. (2008) Enhanced sensitivity of Arabidopsis anthocyanin mutants to photooxidation: a study with fluorescence imaging. *Funct. Plant Biol.* **35**, 714–724.

Sharrock, R.A. and Quail, P.H. (1989) Novel phytochrome sequences in *Arabidopsis thaliana*: structure, evolution, and differential expression of a plant regulatory photoreceptor family. *Genes Dev.* **3**, 1745–1757.

Smyth, D.R., Bowman, J.L. and Meyerowitz, E.M. (1990) Early flower development in Arabidopsis. *Plant Cell*, **2**, 755–767.

Tashiro, S., Tian, C.E., Watahiki, M.K. and Yamamoto, K.T. (2009) Changes in growth kinetics of stamen filaments cause inefficient pollination in *massugu2*, an auxin insensitive, dominant mutant of *Arabidopsis thaliana*. *Physiol. Plant.* **137**, 175–187.

Tatematsu, K., Kumagai, S., Muto, H., Sato, A., Watahiki, M.K., Liscum, E. and Yamamoto, K.T. (2004) *MASSUGU2* encodes Aux/IAA19, an auxin-Regulated Protein that functions together with the transcriptional activator NPH4/ARF7 to regulate differential growth responses of hypocotyl and formation of lateral roots in *Arabidopsis thaliana*. *Plant Cell*, **16**, 379–393.

Timpte, C.S., Wilson, A.K. and Estelle, M. (1992) Effects of the *axr2* mutation of Arabidopsis on cell shape in hypocotyl and inflorescence. *Planta*, **188**, 271–278.

Xu, F., He, S., Zhang, J. *et al.* (2018) Photoactivated CRY1 and phyB interact directly with AUX/IAA proteins to inhibit auxin signaling in Arabidopsis. *Mol. Plant*, **11**, 523–541.

Yang, J., Lin, R., Sullivan, J., Hoecker, U., Liu, B., Xu, L., Deng, X.W. and Wang, H. (2005) Light Regulates COP1-mediated degradation of HFR1, a transcription factor essential for light signaling in Arabidopsis. *Plant Cell Online*, **17**, 804–821.

Yang, C., Xie, F., Jiang, Y., Li, Z., Huang, X. and Li, L. (2018) Phytochrome A negatively regulates the shade avoidance response by increasing Auxin/Indole Acidic Acid protein stability. *Dev. Cell*, **44**, 29–41.e4.

Zhang, Y., Li, C., Zhang, J. *et al.* (2017) Dissection of HY5/HYH expression in Arabidopsis reveals a root-autonomous HY5-mediated photomorphogenic pathway. *PLoS ONE*, **12**, 1–15.